Cytomorphic Electronics With Memristors for Modeling Fundamental Genetic Circuits

Hanna Abo Hanna, Loai Danial, Shahar Kvatinsky, and Ramez Daniel

***Abstract*—Cytomorphic engineering attempts to study the cellular behavior of biological systems using electronics. As such, it can be considered analogous to the study of neurobiological concepts for neuromorphic engineering applications. To date, digital and analog translinear electronics have commonly been used in the design of cytomorphic circuits; Such circuits could greatly benefit from lowering the area of the digital memory via memristive circuits. In this article, we propose a novel approach that utilizes the Boltzmann-exponential stochastic transport of ionic species through insulators to naturally model the nonlinear and stochastic behavior of biochemical reactions. We first show that two-terminal memristive devices can capture the non-linear and stochastic behavior of biochemical reactions. Then, we present the design of several building blocks based on analog memristive circuits that inherently model the biophysical mechanisms of gene expression. The circuits model induction by small molecules, activation and repression by transcription factors, biological promoters, cooperative binding, and transcriptional and translational regulation of gene expression. Finally, we utilize the building blocks to form complex mixed-signal networks that can simulate the delay-induced oscillator and the p53-mdm2 interaction in the cancer signaling pathway. Our approach can provide a fast and simple emulative framework for studying genetic circuits and arbitrary large-scale biological networks in systems and synthetic biology. Some challenges may be that memristive devices with frequent learning and programming do not have the same longevity as traditional transistor-based electron-transport devices, and operate with significantly slower time constants, which can limit emulation speed.**

***Index Terms*—Cytomorphic, cell-inspired circuits, memristors, molecular biology, synthetic biology, systems biology.**

I. Introduction

BIOLOGICAL data sets such as gene expression, proteome, metabolite abundance, and microbiome composition have grown exponentially over the last decade. The analysis of such datasets can provide new insights into biological systems. These insights could play a major role in discovering metabolic pathways related to complex diseases and help in their diagnosis and prevention [1]. However, the analysis of such large amounts of data in a reasonable time, while considering the sophisticated properties of cellular networks, can only be carried out through higher-level biological simulations using high-performance and large-scale computing frameworks [2].

Biological networks exhibit emergent properties such as integration and regulation of noisy graded signals across multiple time scales, through imprecise non-linear components, based on feedforward and feedback loops [3], [4]. As such, the analysis of biological experiments using software-based simulation of cellular networks is a computationally intensive task, especially when the effects of noise are included [2]. For example, in Gillespie algorithm, the most computationally expensive part – the generation of exponentially distributed random numbers, consumes approximately 98% of the processing time [5]–[8]. Recently, efforts have been made to define mathematical tools that can quantify emerging properties of biological systems such as complexity, self-organization, collective behavior of biological swarm and adaptation. Such tools include information theory [9], multifractal analysis [10], energy landscape theory [11] and agent-based systems [12].

Specialized electronic circuits, an area of long-standing and growing interest in engineering, aims to address the challenges of complexity. For example, digital application-specific integrated circuits (ASICs) with a custom analog integrated circuit have been proposed to accelerate the generation of exponentially distributed random numbers [13]. Hardware acceleration techniques that elevate parallelism [14] and special devices to model biological behavior [15] have also been proposed. However, these techniques have a common drawback; the simulation time inevitably increases as the size of the gene and protein networks scales up [5], [6].

Several approaches have been adopted to overcome the challenges of analyzing, modeling and simulating biological networks. For example, emulating the complex behavior of cells has been simplified by assuming digital-logic approximation of genetic circuits [3], [16]. Unfortunately, cells often exhibit stochastic analog behavior rather than purely digital behavior; therefore, the digital approximations are proving to be inadequate [17], and the approximated simulations will not be accurate enough for the prediction of diseases.

Research in the emerging field of *cytomorphic engineering* has tried to overcome the aforesaid challenges using ASICs that exploit the similarities between the physical processes and mathematical models governing chemical reactions and electronics [3], [18]–[23]. Specifically, it has been shown that current

Manuscript received August 19, 2019; revised October 30, 2019; accepted December 14, 2019. Date of publication January 14, 2020; date of current version May 27, 2020. This research was partially supported by the Neubauer Family Foundation, Russell Berrie Nanotechnology Institute NEVET project, EU COST Action IC1401, and the Israeli Ministry of Science and Technology. *(Corresponding author: Hanna Abo Hanna.)*

H. A. Hanna and R. Daniel are with the Department of Biomedical Engineering, Technion-Israel Institute of Technology, Haifa 320003, Israel (e-mail: hanna.abo.hanna2@gmail.com; ramizda@bm.technion.ac.il).

L. Danial and S. Kvatinsky are with the Viterbi Faculty of Electrical Engineering, Technion-Israel Institute of Technology, Haifa 320003, Israel (e-mail: danial.loai@gmail.com; shahar@ee.technion.ac.il).

Color versions of one or more of the figures in this article are available online at https://ieeexplore.ieee.org.

Digital Object Identifier 10.1109/TBCAS.2020.2966634

flow in transistors operated in the subthreshold regime can quantitatively model the fundamental molecular circuits via log-domain translinear circuits based on the Boltzmann exponential distribution [19]. Such an approach can model deterministic and stochastic biochemical reactions because the flows of molecules and electrons current are both driven by the Poisson process. In addition, the emulation time of cytomorphic chip is independent on the number of reactions [23], while the software simulation time is strongly dependent on reactions size [5].

It has been shown that the signal-to-noise ratio (SNR) at the output of the cytomorphic circuit is proportional to the capacitor size and the current levels; therefore, by adjusting the capacitors or currents, any desired SNR can be achieved. However, cellular noise levels in the case of a relatively small number of molecules can be high enough such that extremely low currents and small capacitors are needed. Transistors operating in the subthreshold regime cannot reliably be controlled to adjust such noise levels (due to factors such as body effect, leakage current, or device mismatches). Therefore, to capture highly random fluctuations in genetic circuits that involve low protein concentrations, e.g., DNA-protein binding reactions, it was necessary to design and build standalone artificial noise-generation circuits.

Artificial noise can be generated either using an *ex situ* pseudo-random number generator [20] or by amplifying the intrinsic thermal noise in analog transistors [23]. Significant area consumption can occur because of digitally programmable SRAM and shift registers in these circuits. Thus, cytomorphic circuits would benefit from more efficient analog memory elements that can also naturally compute in an analog and stochastic fashion.

In this paper, we utilize the physical properties of two-terminal memristive devices to mimic the deterministic dynamics and stochastic fluctuations of biochemical reactions and genetic elements. Memristive devices are electrical non-linear passive nano-scale devices that can retain a state of internal resistance based on the history of the applied voltage and the current flowing through them [24], [25]. In the last decade, memristive devices have been proposed in a broad range of applications, including but not limited to resistive random-access memory [26], efficient and highly scalable artificial memristive synapses [27] and neurons [28], supervised and unsupervised learning architectures [29], boolean logic gates [30], programmable analog circuits [31] and high speed true random number generators (couples of nano-seconds for 100 pulses) [32], [33].

Memristive devices and biochemical binding reactions can be seen as analogous in terms of biophysical dynamics and energy [34], [35]. Both have an input-output transfer function with a non-linear behavior, and both are controlled by time-dependent internal state variables. The two logic states of a digital memristor can represent the two states of biochemical reactions; binding and unbinding of protein-DNA or substrate-enzyme. The dynamics of the enzymatic reaction and the forming of a new complex follow the Poisson distribution, as do the dynamics of switching a memristor. We expect that the "cytomorphic" mapping between cellular biology and memristors can be capitalized upon to design a fast and simple emulation framework for building and simulating biological systems [3], [18]–[23],

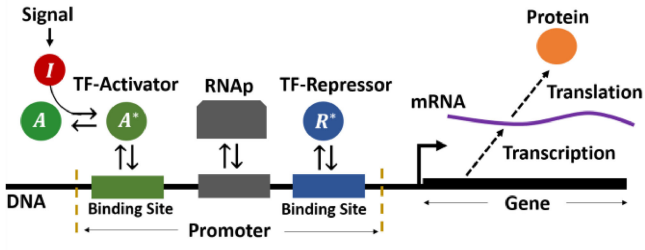

Fig. 1. A simplified overview of the processes in the central dogma, including induction, transcription factor binding, transcription and translation in a bacterial genetic circuit.

[36]. Self-organization and collective behavior of biological components [10] might be modeled by using a diffusor circuits that are widely used to demonstrate silicon retina [37]. We expect that interpolating negative feedback loops and memristors in cytomorphic circuits can mimic adaptation in biological systems. Cytomorphic circuits can also map architectural concepts and design principles from cells to electronics. Living cells have the ability to perform complex, real-time and highly sensitive tasks and process environmental input signals with highly noisy and imprecise parts, such that reliable outputs are produced. These properties make them the ultimate candidate for designing noise-tolerant, ultra-low power electronic systems. Another important advantage of using memristor-based cytomorphic circuits is that it includes both memory and processing in the same computing unit, in analog fashion to biological systems. Therefore, we expect that memristor-based cytomorphic circuits could greatly benefit from lowering the area of the digital memory via memristive circuits.

For readers unfamiliar with genetic circuits, we provide a simplified summary of the processes in the central dogma, how proteins are regulated and produced in living cells in response to cellular signals. Fig. 1 gives an overview. Genes are a stretched sequence of DNA, which encodes the information needed to produce a protein. RNA polymerase (RNAp) is a multi-protein complex that binds to a region of DNA called a promoter and converts the information into messenger RNA (mRNA) in a process called transcription. mRNA is then translated into amino acids, in a process called translation by another complex molecular machine, the ribosome. Amino acids are then converted into proteins. Promoters regulated by RNAp only are constitutive: the rate at which the gene is transcribed, the number of mRNAs produced per unit time, is constant. Other promoters can be regulated by proteins, also known as transcription factors (TF in Fig. 1), which bind their DNA binding site within the promoter. If the transcription factor is an activator, it will enhance the binding of RNAp to the promoter; therefore, it will increase the transcription rate. If the transcription factor is a repressor, it will prevent the binding of RNAp, reducing the transcription rate as a result. TF is usually designed to transit rapidly between the active and inactive form, at a rate that is modulated by chemicals and small molecules called inducers (I in Fig. 1) as well as by environmental signals (e.g., temperature and pH, or receptors).

This paper is organized as follows. In Section II, we introduce the principles and the motivation for modeling biochemical

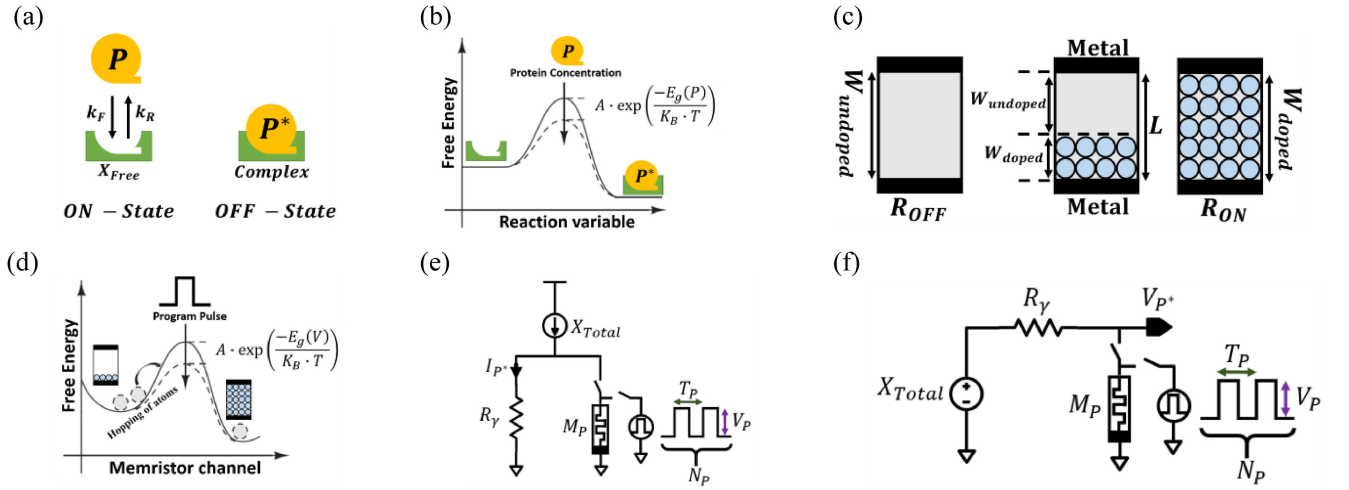

Fig. 2. (a) Cartoon diagram of binding reaction between protein and its target. The reaction can be represented as a two-state system: $ON - state$ representing the free proteins and free binding sites, and $OFF - state$ representing the formation of complex P^* or occupied binding sites. (b) Energy flux of molecules in chemical reactions. (c) Diagram of memristor built in metal-insulator-metal structure. On the left, memristor with highest resistance (R_{OFF}), in the middle intermediate resistance, and on the right, lowest resistance (R_{ON}). (d) Energy flux and flow of ionic species in memristive devices. (e) Memristor based KCL circuit to model the binding reaction between a protein and its target (binding site) in steady state. The current source X_{Total} models all the binding sites and the current through M_P models the occupied binding sites (complex P^*). The pulses are an example of programming pulses used to program the memristor. (f) Memristor based KVL circuit to model the binding reaction in steady state. The voltage across M_P models the occupied binding sites.

reactions with memristive devices. In Section III and Section IV, we discuss the building blocks of our cytomorphic circuits, including gene regulation, transcription, translation, and noise. In Section V, we show a proof-of-concept circuit capable of modeling two genetic circuits, the delay-induced oscillator, and the p53-mdm2 interaction in the p53 pathway. Finally, Section VI concludes with a brief discussion of the potential benefits and future directions of this work.

II. Memristors Model Biochemical Reactions

To map biochemical reactions to memristive devices and vice versa, our first step is to explore both systems in the context of their basic mathematical representation models, kinetics and energy levels.

A. Biochemical Reactions

A simple biochemical reaction that describes the binding of proteins to their targets is illustrated in Fig. 2(a). The targets can be DNA binding sites or other proteins. When proteins bind to their target, a new complex is formed. According to mass-action kinetics, the rate of complex formation is proportional to the collision rate k_F [4]. Consequently, the rate of change of the complex P^* can be described as:

$$dP^*/dt = k_F \cdot X_{Free} \cdot P, \tag{1}$$

$$X_{Free} + P^* = X_{Total}, \tag{2}$$

where X_{Total} represents the total concentration of binding sites, P and X_{Free} represent the concentration of free proteins and free binding sites, respectively.

Equation (1) describes the chemical kinetics rate and (2) can be viewed as a molecular balance law. According to (2), biochemical reactions consist of free and occupied binding sites, which can be viewed as time-dependent internal state variables whose sum is constant. This fraction is controlled by the complex P^*. The rate coefficient of such biochemical reactions is exponential in terms of free energy difference (Gibbs energy [38]) and is often described by the Boltzmann statistics [3]. The reaction can be accelerated by adding catalysts known as enzymes to the system. The enzymes decrease the activation energy and speed up the rate as shown in Fig. 2(b) [4]. A simple solution to (1) and (2) at steady state reveals that the concentration of P^* can be viewed as two logic levels: zero, marked as ON – state and P^* marked as OFF – state, as illustrated in Fig. 2(a).

Biochemical reactions often consist of two simultaneous reactions: a forward reaction with a rate k_F that enhances the reaction and a reverse reaction with a rate k_R that dissociates the complex (Fig. 2(a)) [4]. The kinetics of P^* is thus described as:

$$dP^*/dt = k_F \cdot X_{Free} \cdot P - k_R \cdot P^*. \tag{3}$$

Equations (2) and (3) are the elementary model that captures the kinetics of biochemical reactions, such as the binding of the enzyme to the substrate and the binding of the protein to DNA sites [4]. At steady state, the complex concentration is:

$$P^* = X_{Total} \cdot \frac{P}{P + K_D}, \tag{4}$$

where $K_D = k_R/k_F$ is known as the dissociation constant and has units of concentration. Equation (4) is known as Michaelis–Menten kinetics (MM) in the context of enzyme-substrate binding and it can also describe the binding reaction of proteins to DNA.

B. Memristive Devices

A memristive device is essentially a two-terminal electronic device whose conductance is modulated by controlling the flux or charge passing through it. Such devices are often built in a metal-insulator-metal structure as shown in Fig. 2(c) [25]. A popular abstraction for the insulation region with a length of L is by separating it to doped and undoped regions, marked as W_{doped} and $W_{undoped}$, respectively. If the doped region extends to full-length, the resistivity of the device (also known as the memristance) is dominated by a low resistivity region with a boundary resistance known as R_{ON} (Fig. 2(c), right). If the undoped region extends to the full-length, the total resistivity of the device is dominated by a high resistivity with a boundary resistance R_{OFF} (Fig. 2(c), left).

A simple behavioral model which represents a voltage-controlled memristive system is:

$$v = M\left(W, v\right) \cdot i \tag{5}$$

$$dW/dt \ = \mu \ \cdot \left(\frac{V - V_{TH}}{V_{TH}}\right)^{\alpha} \cdot f\left(W\right). \tag{6}$$

Here, (5) is the linear $I-V$ equation for a resistive device, also known as Ohm's law, where M is the memristance and W is an internal state variable. Equation (6) describes the kinetics of the state variable W, where μ is a constant with units of m/sec, α is a fitting non-linearity constant, V_{TH} is a threshold voltage for programming, V is the applied voltage, and $f(W)$ is a window function adding non-linear dependence on the state variable and solving the mathematical condition at the range edges $W \in (W_{ON},\ W_{OFF})$ [39].

The *I-V* characteristic of memristive devices often exhibits exponential dependency on their state variables [40], with memristance:

$$M_E = R_{ON} \cdot \exp\left(\lambda \cdot W/W_{OFF}\right), \tag{7}$$

where $\lambda = \ln(R_{OFF}/R_{ON})$ is a constant [39]. Alternatively, for the linear *I-V* characteristic in terms of W [27], the memristance is expressed as:

$$M_L = (R_{OFF} - R_{ON}) \cdot W/W_{OFF} + R_{ON}. \tag{8}$$

The *I-V* characteristics in (7) and (8) model memristors with multiple states, acting as an analog device. In addition, they can be used to model the special case, when memristor has only two states and acts as a digital device.

Both biochemical reactions and memristive devices involve the motion of charged atomic or molecular species, including state variable dependency on time (P^* in (3) and W in (6)). The hopping of atoms in memristive devices [41] is analogous to the diffusion of a reactant in biochemical reactions. Both systems are non-linear with two asymptotic values. The two boundary resistance values, R_{ON} and R_{OFF}, which are set by the two boundaries W_{ON} and W_{OFF}, are equivalent to the free and occupied binding sites, respectively. A memristor with two states can model the digital approximation of the biochemical reaction given in (1) and (2). The switching rate in memristive devices follows the Boltzmann statistics and is determined by bias-dependent activation energy [42]. An increase in the effective programming voltage V reduces energy barriers as shown in Fig. 2(d). Thus, the number of applied pulses affects the state of the memristors similarly to the way the number of enzymes affects biochemical reactions. The time required to form a new chemical complex and the delay time of switching memristors both follow a Poisson distribution [42], [43]; thus, the stochastic dynamics for biochemical reactions and memristor switching are similar.

The thermodynamic Boltzmann exponential equations that describe ion flow in memristive devices are strikingly similar to the thermodynamic Boltzmann exponential equations that describe molecular flux in chemical reactions, as can be seen in the following:

$$\psi - \psi_0 = KT \cdot \ln\left(P/P_0\ \right), \tag{9}$$

$$W - W_0 = L/\lambda \cdot \ln\left(M_P/R_{ON}\right), \tag{10}$$

where ψ is the chemical potential, i.e., the Gibbs free energy per molecule [38], which sets the molecule concentration P. W_0 and P_0 are constants referred to as the reference concentration and reference chemical potential, respectively. Equation (10) was derived from (7). The analogy between (9) and (10) suggests that the chemical potential can be encoded as the state variable of the memristor and the protein concentration by the memristance. The above-mentioned analogies suggest that hybrid memristor-CMOS electronic circuits can efficiently model large-scale genetic-processing systems in biological networks.

C. Modeling Michaelis–Menten Kinetics With Memristor-Based Circuits

Multi-state memristors are more suitable for capturing the analog behavior of the biochemical reactions given by (2) and (3), or the steady-state solution in (4). A simple way to model (4) is based on Kirchhoff's current and voltage laws (KCL and KVL). Fig. 2(e) shows a current divider between memristor M_P with a value of P and a resistor with a value of K_D. The circuit can model (4) with X_{Total} representing the total number of binding sites and the complex P^* as the current passing through the resistor. Equation (4) can also be modeled by a KVL circuit, where current dividers are replaced by voltage dividers as shown in Fig. 2(f). Consequently, X_{Total} becomes a voltage source and P^* is modeled by the voltage drop on the memristor.

By substituting (7) in the voltage divider expressions, the dropping voltage across M_P can be represented as:

$$\begin{aligned} P_V^* &= X_{Total} \cdot \frac{M_P}{M_P + \ R_\gamma} \\ &= X_{Total} \cdot \frac{R_{ON} \cdot \exp\left(\lambda \cdot W/W_{OFF}\right)}{R_{ON} \cdot \exp\left(\lambda \cdot W/W_{OFF}\right) + \ R_\gamma}, \end{aligned} \tag{11}$$

where $K_D = R_\gamma$ is analogous to the dissociation constant and M_P is analogous to P in (4). The value of K_D can be easily modified by changing the resistor R_γ. A similar representation can be achieved by current and a KCL circuit. Therefore, the complex P^* can be measured as the current P_I^* or voltage P_V^*, depending on the circuit used. Notably, for $W = 0$, a leakage voltage (or

current) is built in. This is known as the basal level often found in biochemical binding reactions [4]. For $W = W_{OFF}$, a maximal voltage (or current) is built in, representing the negative feedback and the saturation in (3) and (4) due to the forward and reverse reaction.

In specific conditions, when the memristor exhibits linear dependency on the state variable and $f(W) = 1$, programming the device with N_P pulses with a width of T_W and amplitude $A_V > V_{TH}$ changes the memristance according to:

$$M_P = R_{ON} + R_0 \cdot N_p, \tag{12}$$

where $R_0 = (R_{OFF} - R_{ON}) \cdot (\mu/L) \cdot (T_W/V_{TH}) \cdot (A_V - V_T)$.

By substituting (12) in the voltage (or current) divider expressions, (11) is replaced with the following relation:

$$P^*_{V/I} = X_{Total} \cdot \frac{N_p}{N_p + K_D} + X_{Total} \cdot \frac{R_{ON}}{N_p + K_D}, \tag{13}$$

where $K_D = R_{ON}/\mathrm{R}_0 + R_\gamma/\mathrm{R}_0$ is analogous to the dissociation constant, and N_p is analogous to P in (5), which denotes the total number of proteins available for binding. The left-hand term in (13) fits the model of the biochemical binding reaction in (4), and the right-hand term is a leakage current (or voltage) that fits the basal level of promoters and enzymatic reactions. Further analysis and simulation results of an ideal memristor with a linear dependency on the state variable are presented in our previous works [34], [35].

III. Modeling Gene Regulatory Circuits With Memristor-Based Circuits

Computation and processing in living cells are achieved by the regulation of complex gene networks. The input signals that carry the cellular information control the activity of transcription factors such as activators and repressors. While the binding of RNAp to the promoter site initiates the transcription process, the rate of the process is controlled by the number of binding sites bound by the transcription factor [4]. In this section, we introduce different circuits based on memristive devices to model activation and repression processes, hybrid promoters, cooperative binding, transcription, and translation.

A. Activator Binding

In activation, the rate of transcription is proportional to the probability that an activator A is bound to its DNA binding site D. Some activators function (in the sense that they can bind DNA) only when a specific input signal S_X is present [4]. In practice, the signal S_X is a small molecule called an inducer, which binds the activator to form a complex $[AS_X]$. Correspondingly, this reaction can be described by MM kinetics with a forward rate k_F and reverse (dissociate) rate k_R. Biochemical reactions such as the binding of small molecules to transcription factors are usually fast, with a sub-second timescale, as compared to other biological processes, such as protein expression [4]. Therefore, and for simplicity, in this work we assume that these reactions are in their steady state. According to (4), the complex $[AS_X]$ is given by:

$$[AS_X] = A_T \cdot \frac{S_X}{S_X + K_{A-S_X}}, \tag{14}$$

where $[AS_X]$ is the function activator, A_T is the total number of activators, and $K_{A-S_X} = k_R/k_F$ is the dissociation constant.

The binding of the complex $[AS_X]$ to the DNA binding site D often reaches equilibrium in seconds, while transcription and translation of the gene takes minutes [4]. Therefore, the binding of complex $[AS_X]$ to DNA can also be described by MM kinetics:

$$[AS_X D] = D_T \cdot \frac{[AS_X]}{[AS_X] + K_{AS_X - D}}, \tag{15}$$

where $[AS_X D]$ is the fraction of DNA sites bound by $[AS_X]$, D_T is the total number of binding sites, and K_{AS_X-D} is the dissociation constant. Equation (15) is a function of the signal S_X through the complex $[AS_X]$; therefore, the current or voltage representing $[AS_X]$ from (14) must be converted to proper programming voltage to set the memristance $[AS_X]$ in (15).

The promoter activity is computed as the probability that the DNA binding site D is occupied by a functional activator. Transcription cannot initiate if RNAp is not bound to the promoter, regardless of whether the activators bind. Therefore, in our model, we multiply the promoter activity by a factor β, which models the fraction of promoter sites bound by RNAp. Thus, we express the promoter activity by:

$$f_A\left(AS_X, RNAp\right) = \beta \cdot [AS_X D]\,. \tag{16}$$

Note that when no signal is present, there is a very small probability that RNAp will bind and transcribe the gene, which in turn leads to the basal level, $f_A([AS_X] \approx 0)$. This leakage is modeled by the low resistance of $[AS_X]$ in (15).

Fig. 3(a) shows a memristor-based KVL circuit that models the activity of a biological promoter, as given in (16). The KVL circuit models the binding of the complex $[AS_X]$ to the DNA binding site D, as given in (15). Transistor M_0 converts the voltage $[AS_X D]$ to a current through the transconductance g_{M_0}. The circuit output is a voltage which is dropped on the memristor M_{RNAp}, which represents the promoter activity given in (16). The voltage source D_T was chosen to be -200 mV to fit the small signal dynamic range of the PMOS transistor M_0. The memristor M_{RNAp} can model the activity of RNAp using two states: high resistance to model the binding of a high level of RNAp and set β to a high value, and low resistance to model the binding of a basal level of RNAp and set β to a low value in (16). The purpose of the memristor M_{RNAp} is to capture the stochastic dynamics of RNAp, as will be discussed in Section VI. The memristor M_{RNAp} is programmed to high resistance ($W = 0.5 \cdot W_{OFF}$) when a "Bias" pulse, which is accompanied by random small pulses, is applied, as shown in Fig. 3(a).

SPICE and MATLAB simulation results for the activation process are shown in Fig. 3(b-c). Fig. 3(b) shows the non-linear monotonic transfer function, which results from binding activators to the DNA binding site. Fig. 3(c) shows a linear monotonic curve that describes the transfer function of the promoter activity

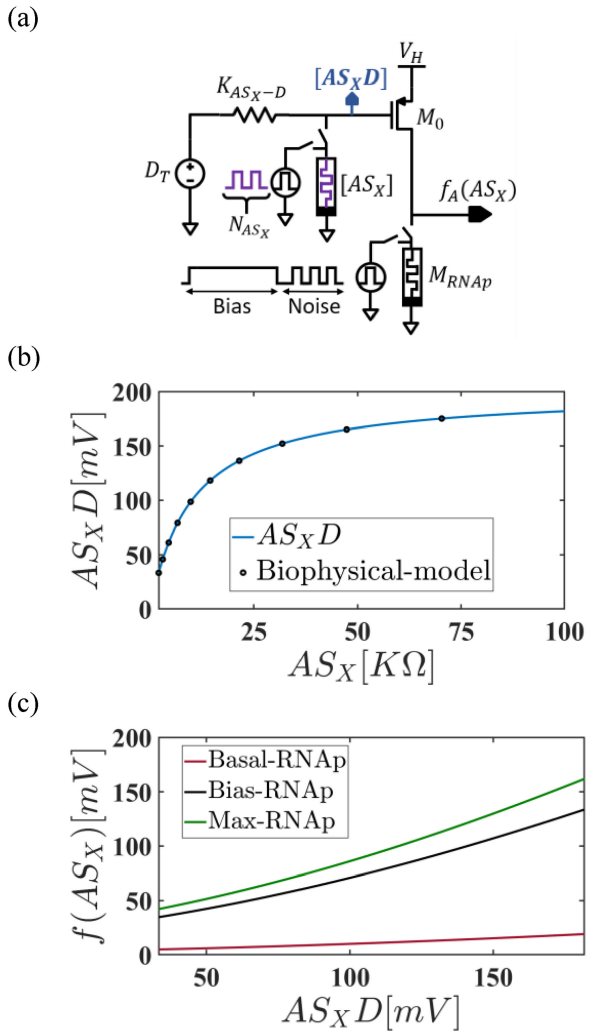

Fig. 3. (a) Two-stage memristor based circuit to model the activation process. The KVL circuit models the binding of a function activator to its DNA binding site. Programming M_{RNAp} models the binding of RNAp to the promoter to initiate transcription. (b) SPICE and MATLAB of binding reaction between the function activator and DNA site. The solid curve is SPICE data and the dotted curve is the biophysical model (MATLAB) given in (15). (c) SPICE simulations of promoter activity $f(AS_X)$. The red curve (Basal) represents the binding of a basal level of RNAp ($M_{RNAp} = R_{ON}$). The black (Bias) and the green (Max) curves model the binding of a high or maximal level of RNAp ($M_{RNAp} = R_{ON} \cdot exp(\xi \cdot \lambda)$ where $\xi = [0.5,\ 0.55]$, respectivley).

and complex level when a high level of RNAp is bound (RNAp-bias and RNAp-max) and weak dependency when a basal level of RNAp is bound.

For the design of the proposed circuits, we used a 0.18 μm CMOS process, and memristors fitted by the VTEAM model [39], [44] to the Pt/HfOx/Hf/TiN RRAM device with a buffer layer [45]. This device has a high-to-low resistance state ratio of $\sim$50 and low forming, set, and reset voltages. Circuit and memristors parameters are listed in Table I.

B. Repressor Binding

Repressors are transcription factors that can bind a specific DNA site H in the promoter [4]. When the site H is free (not occupied by a repressor), RNAp binds the promoter and transcribes the gene, but if the site is occupied by a repressor, RNAp cannot bind and no transcription is obtained. Based on a similar explanation as above, the binding of repressor R to site H at steady state is described by:

$$[RH] = H_T \cdot \frac{R}{R + K_{R-H}}, \tag{17}$$

where $[RH]$ is the fraction of bound DNA sites, H_T is the total number of binding sites, and K_{R-H} is the dissociation constant.

The sum of the free and occupied binding sites is equal to the total number of binding sites; therefore, we can describe the concentration of free DNA binding sites as:

$$H = H_T - [RH] = H_T \cdot \frac{K_{R-H}}{R + K_{R-H}}. \tag{18}$$

Given that the sum of probabilities that a binding site is occupied or free is equal to one, we can describe the activity of a promoter that is controlled by a repressor as:

$$f_{\mathrm{R}}\left(R, RNAp\right) = \beta\left(RNAp\right) \cdot H. \tag{19}$$

Fig. 4(a) shows a memristor-based circuit that models promoter activity of the repression process. The circuit models the binding of the repressor R to the DNA binding site and the output $[H]$ represents the free binding sites as given in (18). In this case, RNAp binds only if the site H is free; therefore, our model assumes that the bias is 'zero' when the promoter is occupied by a repressor, and "high" when the promoter is free. SPICE and MATLAB simulation results are shown in Fig. 4(b-c). Circuit and memristor parameters are listed in Table I.

C. Hybrid Promoter

In eukaryotic cells, promoters are often controlled by combinatorial transcription factors [4], [16], [46]. Each transcription factor has a binding site with a specific DNA sequence; therefore, such promoters have multi-binding sites and are called hybrid or combinatorial promoters. A promotor regulated by an activator and a repressor is one example of a synthetic bacterial hybrid promoter prevalent in biotechnological applications. Such a promoter has four statistical states: free binding sites $[V]$, binding sites occupied by an activator $[VA]$, binding sites occupied by a repressor $[VR]$, and $[VAR]$, where both A and R bind to the binding site V, as shown in Fig. 5(a).

Transcriptional events occur mainly from the state $[VA]$, in which the only activator A binds. Here we assumed that there is no crosstalk between the binding reactions of the activator and the repressor. As such, the hybrid promoter activity is given by:

$$f_H = D_T \cdot \frac{\left(\frac{A}{K_A}\right)^{n_1} + \left(\frac{A}{K_A}\right)^{n_1} \cdot \left(\frac{R}{K_R}\right)^{n_2}}{1 + \left(\frac{A}{K_A}\right)^{n_1} + \left(\frac{R}{K_R}\right)^{n_2} + \left(\frac{A}{K_A}\right)^{n_1} \cdot \left(\frac{R}{K_R}\right)^{n_2}}. \tag{20}$$

This function can be approximated by the simple "logic" function $(A \cdot \bar{R})$, with three plateau levels: the basal level, when A is not bound and R is bound, the maximum activity level, when A is bound and R is not bound, and the intermediate activity level, when both A and R are bound [4]. Fig. 5(b) shows the simulation results of (20). The four labeled points (X, Y, Z, W)

TABLE I
CIRCUIT AND MEMRISTORS PARAMETERS

Symbol	Quantity	Value	Symbol	Quantity	Value
D_T	Total DNA binding sites for activator	$-200[mV]$	A_R	Noise pulse amplitude	$1[V]$
H_T	Total DNA binding sites for repressor	$-200[mV]$	T_R	Noise pulse period	$12[nsec]$
K_{AS_X-D}	Dissociation constant for activator-DNA binding	$10[K\Omega]$	I_{DC}	Current source	$40\mu[A]$
K_{R-H}	Dissociation constant for repressor-DNA binding	$10[K\Omega]$	$Q_1 - Q_2$	Differential amplifier transistors	$\frac{W}{L} = \frac{2\mu m}{2\mu m}$
K	Dissociation constant for hybrid promoter	$10[K\Omega]$			
K_D	Dissociation constant for cooperative binding	$10[K\Omega]$	$Q_3 - Q_4$	Load transistors	$\frac{W}{L} = \frac{18\mu m}{2\mu m}$
V_H	Voltage source	$0.5[V]$			
$(W/L)_0$	Size of transistor M_0	$5\mu m/1\mu m$	Q_5	Common source (CS) amplifier transistor	$\frac{W}{L} = \frac{80\mu m}{1\mu m}$
R_{ON}	Lowest memristance achieved when $W = 0$	$2[K\Omega]$			
R_{OFF}	Highest memristance achieved when $W = W_{OFF}$	$100[K\Omega]$	R_S	Feedback resistor	$2[K\Omega]$
μ	Memristor constant	$2.8[mm/sec]$	R_X	Resistor	$72[K\Omega]$
$\lvert V_{TH}\rvert$	Memristor threshold for programming	$0.4[V]$	R_D	Load Resistor	$14[K\Omega]$
α	Fitting constant	1	R_F	CS Feedback resistor	$3[K\Omega]$
$f(\cdot)$	Window function	1	V_{DD}	Voltage source	$1.8[V]$

represent the boundary cases (digital behavior) of (20). Point X represents the case where the site is unoccupied by either activators or repressors (state $[V]$), point W represents the case where a high level of repressor binds their DNA binding sites (state $[VR]$), point Y represents the case where a high level of activator binds their DNA binding sites (state $[VA]$) and point Z represents the case where activators and repressors bind the DNA binding sites (state $[VAR]$). In the simulation of (20), the property whereby the binding of the repressor blocks the attachment of RNAp to the promoter was not taken into account; therefore, the simulation shows that $f_H(Z)$ is higher than $f_H(X)$ and $f_H(Y)$ instead of being near the basal (low) level (point W).

The implementation of a hybrid promoter is shown in Fig. 5(c). The circuit functions as a fuzzy AND gate and it contains two memristors, X and Y, which model the activator and the repressor binding sites, respectively. Initially, memristors X_A and Y_R are both programmed to low resistance, which models the free activator and the occupied repressor binding sites, respectively. Such an arrangement results in the smallest equivalent resistance and the lowest promoter activity. Programming X_A to high resistance models the binding of the activators and doing the same for Y_R models the unbinding of the repressors. This arrangement results in the highest equivalent resistance and the maximum promoter activity. Simulation results are shown in Fig. 5(c). The four labeled points are the complements of those in Fig. 5(b).

D. Cooperative Binding

Cooperative binding in living cells can be described as the number of identical components that collectively interact to enhance and stabilize biochemical reactions [4]. Transcription factors are often composed of several identical subunits, such as dimers or tetramers; therefore, proper functionality is achieved when the subunits bind together. In our previous work, we presented a memristor based circuit to model cooperative binding. The Hill coefficients were encoded as the programming pulse width. The models were based on the correlation between the memristance and the pulse width: applying a longer positive (negative) pulse results in a larger increase (decrease) of memristance [27], [47]. Mathematical analysis and simulation results can be found in [34], [35].

IV. NOISE IN GENETIC CIRCUITS

Biological systems are inherently stochastic. The transportation of discrete random carriers is accompanied by collisions and probabilistic arrival, which generate random fluctuations. These fluctuations, known as intrinsic noise through networks, are well modeled as a Poisson process, generating shot noise which scales as the square root of the molecular count [4], [48]. An example of such a process is the stochasticity in gene expression in genetically identical cells, which arises from fluctuations in transcription and translation.

The fluctuations of protein often originate from the random production and decay of low-copy mRNAs. Several models were proposed to describe the stochasticity in protein levels. Two well-known models are the "Poisson scenario" and the "telegraphic" model [49]. In the "Poisson scenario" constant promoter activation is assumed, and noise is only included in mRNA production and destruction. The "telegraph scenario" assumes that the promoter becomes active only for short bursts, during which transcripts are made and mRNA and protein production follow deterministically.

As the first order of approximation, the expression of mRNA is proportional to the rate of RNAp arrival at the promoter site. The number of RNAp arriving at the promoter is Poisson distributed with a variance that is equal to the mean. In our stochastic model, we assume that each binding of RNAp to the promoter site produces a single mRNA molecule; therefore, the promoter can be viewed as a counter of RNAp. The stochastic kinetics of a pulse counter often follow Poisson shot noise statistics (*e.g.,* photon counting [3]); therefore, the number of mRNAs also follows the Poisson distribution.

To model the stochastic behavior of gene expression, a multilevel (analog) memristor M_{RNAp} is used as a counter of applied programming pulses. If M_{RNAp} exhibits linear dependency on the state variable as in (12), then each programming pulse

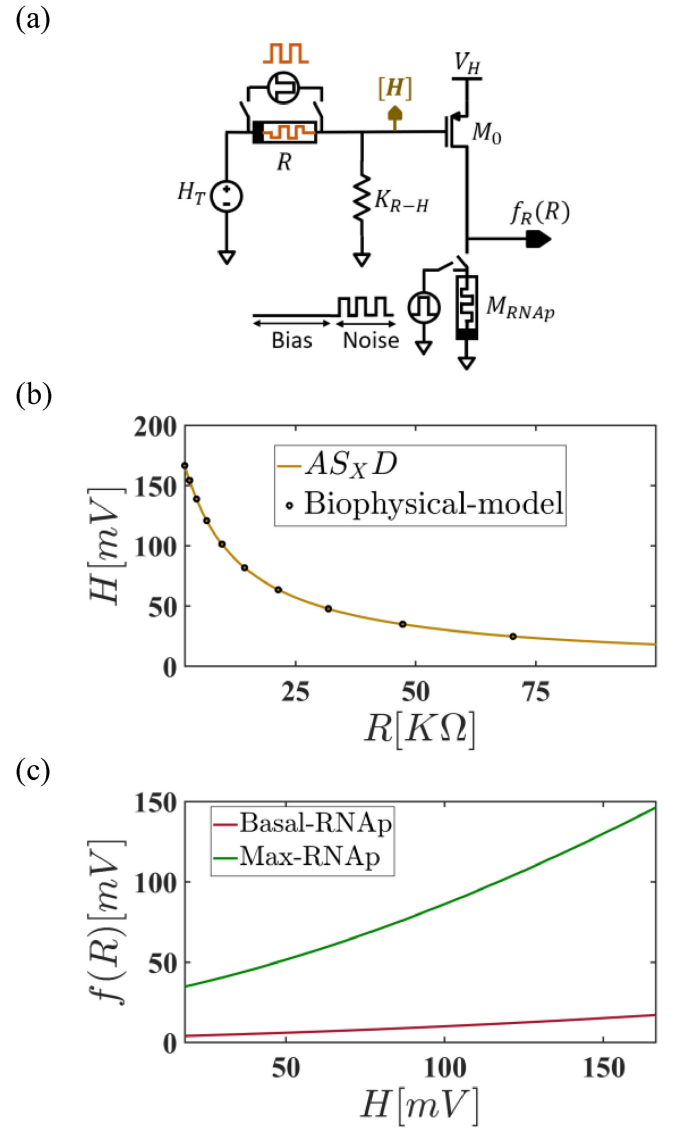

Fig. 4. (a) Two-stage memristor based circuit to model the repression process. The KVL circuit models the binding of a repressor to its binding site. (b) SPICE and MATLAB (biophysical model) simulations of activator binding. H represents the concentration of free DNA sites and R represents the repressor level. The solid curve is SPICE data and the dotted curve is the biophysical model (MATLAB) given in (18). (c) SPICE simulations of promoter activity $f(R)$. Green and red curves are defined as in Fig. 3(b).

models the arrival of one RNAp to the promoter site. To model the probabilistic number of RNAp, the programming pulses (N_R) are controlled by a "random clock. The random clock exhibits Poisson characteristics with mean $\overline{N_R}$ that is equal to the variance $\overline{\Delta N_R^2}$. In cases where M_{RNAp} exhibits exponential dependency on the state variable as in (8), the programming pulses include a bias pulse accompanied by N_R short random pulses.

Here, we linearized the exponential characteristic of the memristor in order to implement a linear counter:

$$M_{RNAp} = M_{RNAp}(w_0) + \delta \cdot M_{RNAp}(w_0) \cdot (w - w_0), \tag{21}$$

where $\delta = \lambda \cdot K_{off} \cdot T_P \cdot \Delta V/(L \cdot V_{TH})$.

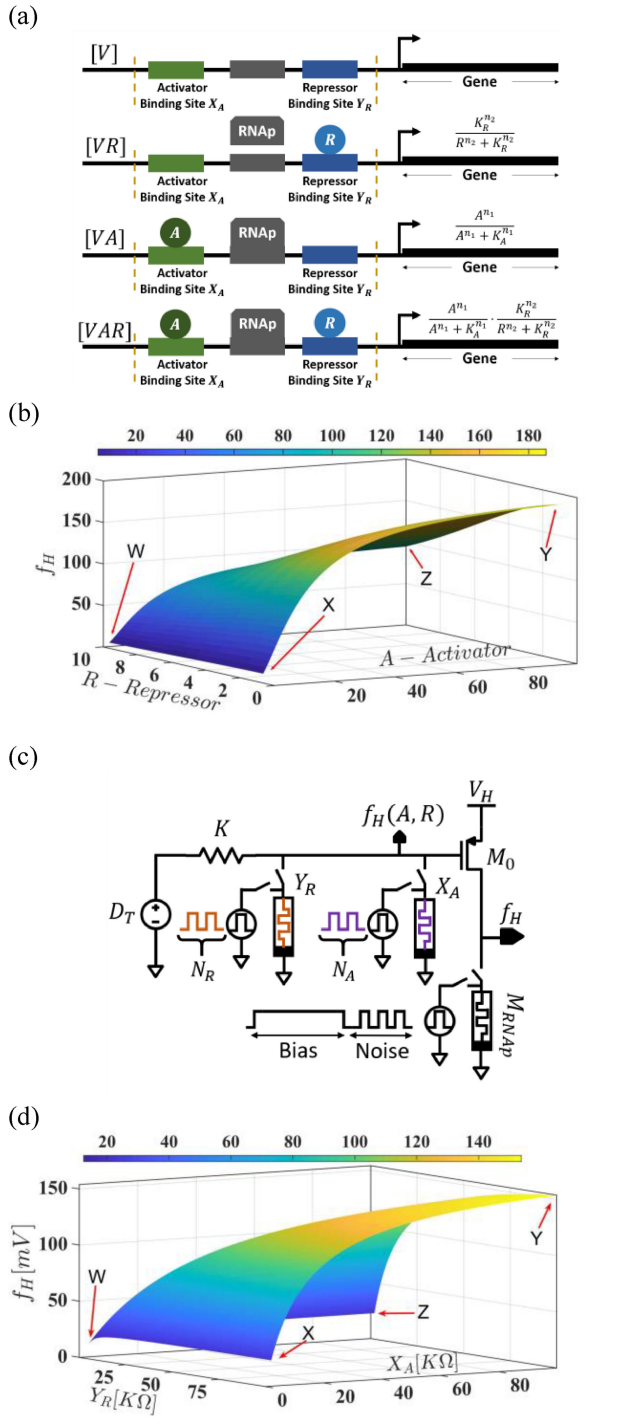

Fig. 5. (a) Diagram of the four states of the hybrid promoter. State $[V]$: DNA binding sites are free from activators and repressors. State $[VR]$: repressor binds the DNA site. State $[VA]$: activator binds the DNA site. State $[VAR]$: both activator and repressor bind the DNA site. (b) MATLAB simulation results of the promoter activity given in (20) [4]. Parameters used in the simulation: $D_T = 200$, $K_A = 15$, $n_1 = 1.5$, $n_2 = 2$ and $K_R = 10$. The four labeled points represent the extreme cases of the hybrid promoter. (c) Two-stage memristor-based circuit to model the hybrid promoter. The memristors X_A and Y_R model the binding sites for the activator and repressor, respectively. Low X_A represents the case where the DNA site is not bound by the activator and high X_A represents the case where the DNA site is bound by the activator. High Y_R represents the case where the DNA site is not bound by the repressor and low Y_R represents the case where the DNA site is bound by the repressor. (d) SPICE simulations of promoter activity f_H using the circuits in Fig. 4(c). The four labeled points represent the extreme cases.

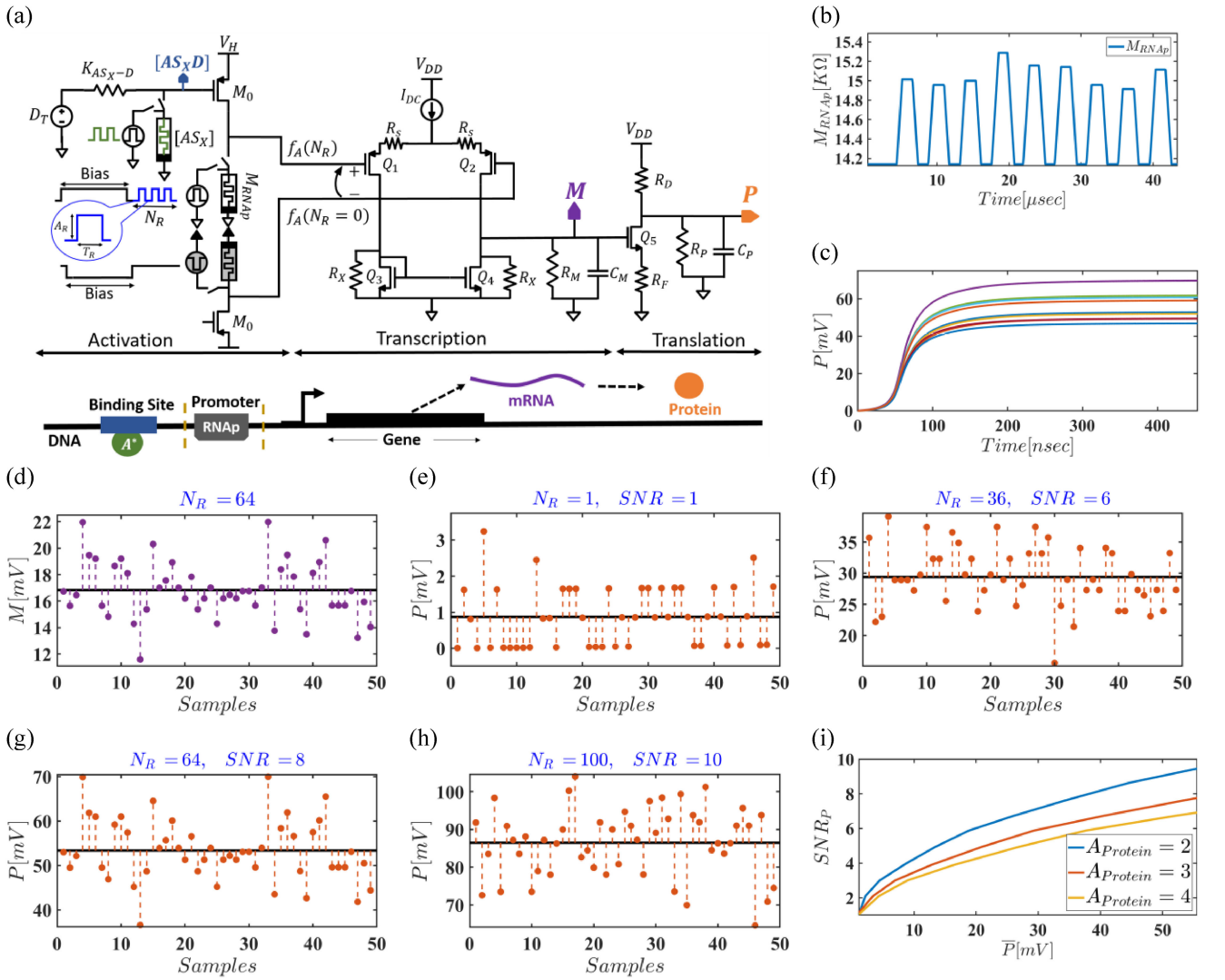

Fig. 6. (a) Memristor-based circuit to capture the deterministic and stochastic behavior of the activation-transcription-translation process. The activation stage models the binding of the function activator to the DNA binding site. The transcription stage models the dynamics of the transcription process in which a segment of DNA is copied into mRNA by the enzyme RNA polymerase (RNAp). The capacitor voltage M is the mRNA level. The translation stage models the dynamics of the translation process by which mRNA is decoded to produce protein. The gain of the common source amplifier captures the Fano-factor $(1 + b)$ in the translation process. The capacitor voltage P is the protein level. The values of $R_{M,P}$ and $C_{M,P}$ are set according to the half-life of mRNA and protein molecules. (b-i) SPICE simulation results of stochastic gene expression. (b) Effect of random number of programming pulses on the memristor M_{RNAp}. Initially, M_{RNAp} is programmed by the bias pulse to $M_{RNAp} = 14.14\,\text{K}\Omega$. Then, a random number of programming pulses is used to add stochasticity to the memristance. The number of pulses (N_R) is Poission distributed with mean of $\overline{N_R} = 64$. (c) SPICE simulation results of the dynamics of the stochastic translation process (protein production) for different values of M_{RNAp}. (d) SPICE simulation results of mRNA production in the transcription process. The violet dots are the steady state output voltage of the transcription stage for fifty Poisson distributed $N_R's$ with mean value of $\overline{N_R} = 64$. The black line is the mean value of mRNA calculated by considering all the dot points. (e-h) SPICE simulations of the translation process for different Poisson distributed programming pulses with mean of $\overline{N_R} = [1,\ 36,\ 64,\ 100]$, respectively. The orange dots are the output voltage of the translation stage with $A_{Protein} \approx 3$. The black line is the mean value calculated by considering all the dot points. (i) SPICE simulation results of SNR versus molecule concentration $(\overline{P})$, for different gains $A_{Protein} = [2,\ 3,\ 4]$, which represent different Fano factors, $\varphi = [1,\ 2,\ 3]$, respectively.

Equation (26) reveals that a memristor can be used as an analog counter around a fixed working point. The first term, $M_{RNAp}(w_0)$, represents the bias that initiates and sets the fraction of promoter sites bound by RNAp (β in (16)). This level ranges from basal to high. Zero bias pulse sets $M_{RNAp}(w_0)$ to low resistance, which models the binding of a basal (low) level of RNAp; then, the transcription level is expected to be low, while non-zero bias pulse sets $M_{RNAp}(w_0)$ to high resistance, which initiates the transcription process and models the binding of a high level of RNAp. The second term in (21) is used as "a noise injection source" by programming with a random number of pulses, N_R.

To include stochastics in the transcription-translation circuit in Fig. 7, we define the input for the transcription stage, f_M, as the difference between $f_M(N_R)$ for any number of pulses N_R and $f_M(0)$ for $N_R = 0$. A simple implementation of this definition is a differential amplifier, where the positive input is $f_M(N_R \neq 0)$ and the negative input is $f_M(N_R = 0)$. The

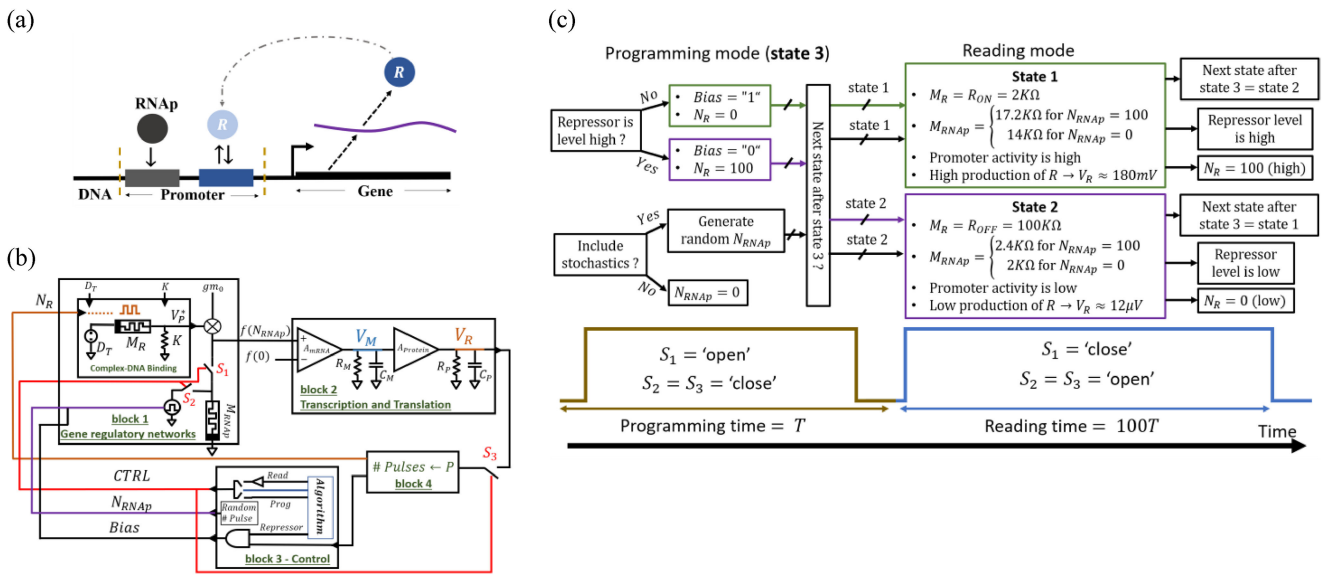

Fig. 7. (a) Cartoon model of the delay-induced oscillator. (b) Block diagram of the circuits used to model the delay-induced oscillator. The control blocks set the connectivity and the input signals for block 1. (c) Time diagram and algorithm used when simulating the network.

inputs $f(N_R)$ and $f(N_R = 0)$ are defined according to the gene regulation circuit, (16) in the activation process and according to (19) in the repression process. For example, in the case of activation the input for the differential amplifier will be:

$$f_M(N_R) - f_M(N_R = 0) = ([AS_X D] \cdot gm_0 \cdot \delta \cdot M(w_0)) \cdot N_R. \quad (22)$$

The noise power of transcription (noted as ψ_M) is defined as the ratio between the variance $\overline{\Delta M^2}$ and the mean $\bar{M}$, and the signal-to-noise ratio (SNR) is defined as the ratio between $\bar{M}$ and the standard deviation $\overline{\Delta M}$. Using (22), the noise power and the SNR of the transcription process can be represented as:

$$\psi_M = \rho \cdot A_{mRNA} \cdot \frac{\overline{\Delta N_R^2}}{\overline{N_R}}, \quad (23)$$

$$SNR_M = \sqrt{N_R}, \quad (24)$$

where $\rho = ([AS_X D] \cdot gm_0 \cdot \delta \cdot M_R(w_0))$ and A_{mRNA} is the gain of the transcription stage.

In an analogy to the transcription process, translation can be viewed as the process of counting ribosomes that arrive at mRNA molecules. Biological experiments and biophysical models have shown that the noise power of translation in protein generation is higher than the noise power of transcription in mRNA generation, $\psi_{protein} > \psi_{mRNA}$. Therefore, the variance in protein generation is larger than the Poisson statistic, $\overline{\Delta P^2} = \varphi \cdot \bar{P}$ [50], where $\varphi = 1 + b$ is known as the Fano-factor. The parameter b is known as the burst size and is equivalent to the number of proteins synthesized from a single mRNA transcript. The burst size originates from the molecular gain between the mRNA copy number and the protein copy number [3], [50]. Using our mathematical analysis in (23) and (24), we can express the noise power of translation as:

$$\psi_P = A_{Protein} \cdot \psi_M, \quad (25)$$

where $A_{Protein} \equiv \varphi = 1 + b$ is the gain of the translation stage.

Fig. 6(a) shows an analog circuit that models the stochastic process of mRNA and protein production controlled by the activator-inducer complex. The circuit comprises the activation, transcription and translation stages. The transcription stage is implemented as a differential amplifier and models the stochastic dynamics of the mRNA level. A capacitor and resistor at the output of the stage were added to model the dynamics of transcription process and set the halftime of mRNA. The translation stage is implemented as a degenerated common source amplifier and models the stochastic dynamics of the protein level. The ratio R_D/R_F sets the gain of the transcription stage, which sets the Fano-factor in (21). The activation stage can be replaced with the circuits in Fig. 3–5, depending on the required functionality.

Fig. 6(b) shows the SPICE simulation results of the dynamics of M_{RNAp} when programmed with a random number of pulses (N_R) and Fig. 6(c) shows the dynamics of protein production in translation process for different values of M_{RNAp}. Fig. 6(d-h) show SPICE simulation results of the stochastic behavior of the transcription and translation stages when applying a different random number of pulses (N_R). In each simulation, fifty random numbers which follow a Poisson distribution were generated by MATLAB with pre-defined mean, width, and amplitude. The pulses were used in programming M_{RNAp} (N_R in (21)) to add small changes in the memristance to emulate the stochasticity in the number of arriving RNAp. Fig. 6(i) shows SPICE simulation results of the impact of different gains on the SNR of the translation process.

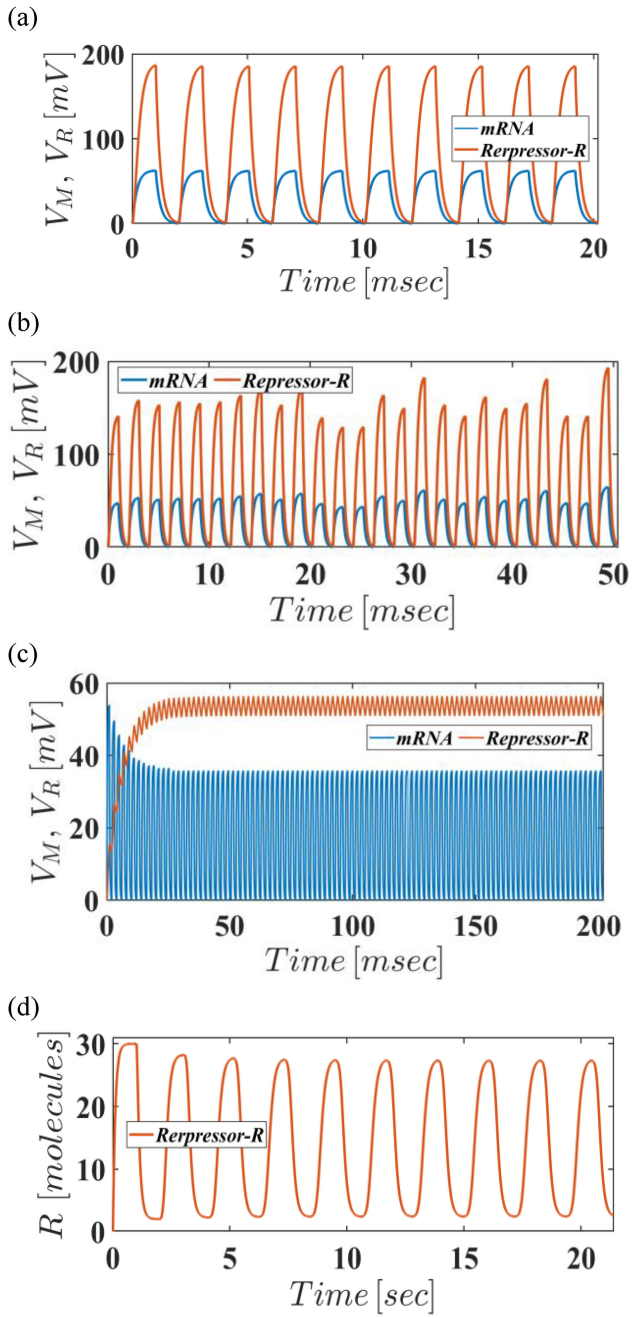

Fig. 8. MATLAB simulation results of the delay-induced oscilator: (a) oscillation without noise ($N_{RNAP} = 0$), (b) oscillation with noise in the number of RNAp (N_{RNAp} is Poisson distributed) and (c) a special case where the half-life of protein is much longer than the half-life of mRNA. In this case the mRNA oscillates, and the protein reaches steady state. (d) MATLAB simulation results of the delay-induced oscillator model in [53]
Source: W. Mather, M. R. Bennett, J. Hasty, and L. S. Tsimring [53]. Copyright 2009 by the American Physical Society.

V. Modeling Genetic Circuits

In this section, we emulated two genetic networks, the delay-induced oscillator [51] and the interaction between p53 and mdm2 in cancer signaling pathways [52]. Both networks employ delay in the negative feedback to implement the genetic clock and synchronization between biological signals.

A. Working Methodology

The building blocks of the networks used to model the genetic networks are based on the gene regulatory, transcription and translation circuits shown above. The connectivity between the blocks is obtained using switches which are controlled by a predefined algorithm. The controlled switches operate the system in two modes, program and read. In programming mode, the switches disconnect the memristors from the circuits and the memristors are programmed by a voltage pulse generator. In reading mode, the switches connect the memristors to the circuits and they function as two-terminal passive devices.

B. Delay-Induced Oscillator

Although the proposed memristor-based circuits are analog in nature, the flexibility in adding digital basis functions such as delays through a control block simplifies the modeling and the simulation of well-known synthetic circuits such as the delay-induced oscillator.

Fig. 7(a) shows a cartoon model of an auto-negative feedback loop circuit, where the gene R represses its own transcription. The time delay between repression and translation causes oscillations in the R level, which can be viewed as charging and discharging of a capacitor [53]. To emulate the genetic oscillator circuit, we configure the building blocks as shown in Fig. 7(b). First, we program the gene regulatory (block 1) model to behave as a repressor (Fig. 4(a)). Second, the output of block 2 (Translation-Transcription) is converted to a number of pulses through block 4 ($\#Pulses \rightarrow P$). Then, it is returned in a feedback loop to the circuit input.

The control block runs the network in two modes (reading and programming) and switches the network between three states as shown in Fig. 7(c). The switches are configured according to the current state. When the system is in reading mode (state 1 or state 2), the switches S_2, S_3 are open and S_1 is closed. Block 1 calculates the promoter activity, which is high if the system is in state 1 and low if it is in state 2. Block 2 receives its input from block 1 and calculates the dynamics of mRNA and protein (transcription and translation) and the final level of the produced protein V_R. The repressor level (V_R) is low if the previous state was 1 and high if the previous state was 2. When the system switches to state 3 (programming mode), the switches S_2, S_3 close and S_1 opens. If the previous state was state 1, the promoter site is bound by a repressor; therefore, RNAp cannot bind. In this case, a large number of pulses (N_P) is generated by block 4, which results in programming memristor M_R to high resistance, then, block 3 sets the bias pulse to zero ($Bias =' 0'$), and results in programming M_{RNAp} to low resistance. If the system was in state 1 (repressor level is low), the promoter site is free; therefore, RNAp can bind. In this case, block 4 generates a small number of pulses (N_P), the memristor M_R is programmed to low resistance, and M_{RNAp} is programmed to low resistance $(Bias =' 1')$. In addition to the bias pulse, a stochastic number of pulses (N_{RNAp}) can be generated and added to include stochastics in the network as shown in Fig. 7(c). The reading time in the network was chosen to be 100x the programming time (Fig. 7(d)) to maintain continuous operation of the circuits. The programming time must be

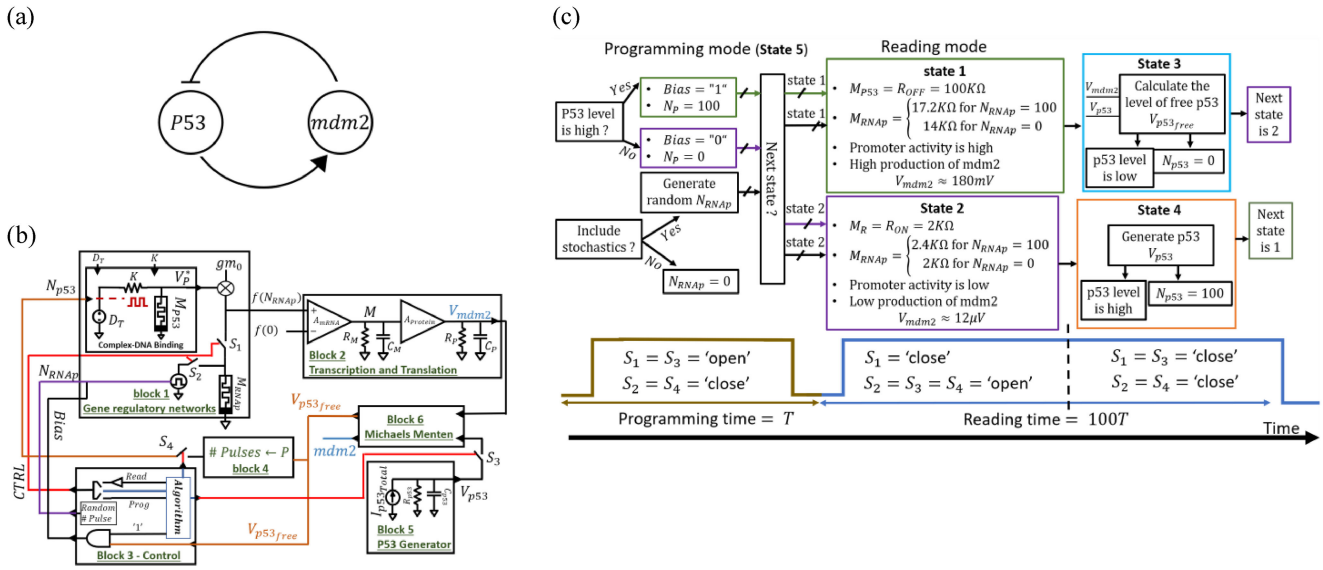

Fig. 9. (a) Cartoon of the p53-mdm2 interaction. p53 activate the transcription of Mdm2, while Mdm2 binds p53 to promote its ubiquitination and degradation. (b) Block diagram of the network used to model the negative feedback loop in p53-mdm2 interaction. The control blocks set the connectivity. (c) Time diagram and algorithm used when simulating the network.

chosen such that all memristors are programmed to their final value. For example, in our models, we chose the programming time to be 10 μsec and the reading time to be 1 msec.

We examine the delay-induced oscillator in three comprehensive cases: 1) oscillation without noise as shown in Fig. 8(a), 2) oscillation with noise as shown in Fig. 8(b), and 3) where no oscillations occur, as shown in Fig. 8(c). Case 3 is a special case where the half-life of the protein is ten times longer than the half-life of the mRNA. For cases (1) and (2), we chose the half-time of mRNA and protein to be 166 μsec (reading time/6) to ensure that the output of block 2 reaches 99% of its final value. We ran 10 iterations for case 1 and 50 iterations for case 2, where each iteration contains programming and reading cycles. In case 3, we chose the half-life of mRNA to be 166 μsec and the protein half-life to be 10 msec. We ran 200 iterations for this case.

For all three cases, the total number of DNA binding sites was set to $D_T = |200\text{ mV}|$, the memristance $M_R \in [2\text{ K}\Omega - 100\text{ K}\Omega]$, where $M_R = 2\text{ K}\Omega$ represents a basal level of the repressor R, and $M_R = 100\text{ K}\Omega$ represents the maximum level of R, achieved when V_R is maximal. The dissociation constant for the repressor binding was chosen to be $K = 10\text{ K}\Omega$, the transconductance $g_{m_0} = 150\ \mu\text{S}$, and the gain of block 2 $A_{mRNA} = 1$ and $A_{Protein} = 3$. The transfer function of block 4 ensures that the maximum value of V_R is converted to $N_R = 100$, and the pulse width T_P ensures that maximum N_R sets the memristance to boundary value R_{OFF}.

Fig. 8(d) shows MATLAB simulation results of the delay-induced oscillator model presented in [53]:

$$\frac{dR}{dt} = \alpha \cdot \frac{C_0}{C_0 + R\,(t-\tau)} - \beta \cdot R - \gamma \cdot \frac{R_0}{R_0 + R}, \qquad (26)$$

where R is the number of repressor molecules, τ is the delay time, α is the production rate of the repressor, β is the rate of degradation due to dilution, R_0 is the dissociation constant for repressor-protease binding, and γ is the maximum rate of degradation due to protease. It can be seen that with proper time and amplitude scaling, our simulation results are compatible with the biological experiments in [51] and the mathematical model in (21) and in [53].

C. P53 Pathway

The p53 network is perhaps the most important pathway involved in preventing the initiation of cancer. The levels of the p53 protein and its activity are upregulated in response to various stresses such as DNA damage and hypoxia. Active p53 initiates different transcriptional programs that result in cell cycle arrest, cellular senescence, or apoptosis. The core regulatory circuit of p53 consists of the protein p53 and the E3 ligase protein, Mdm2. The proteins p53 and mdm2 form a negative feedback loop, in which p53 positively regulates mdm2 by activating Mdm2 transcription and Mdm2 negatively regulates p53 by promoting its ubiquitination and degradation as shown in Fig. 9(a). Negative feedback loops, such as that between p53 and Mdm2, are motifs found far more often than predicted by chance in biological networks. Therefore, we show as a proof-of-concept the ability of our circuits to simulate the negative feedback loop between the tumor suppressor p53 and the oncogene Mdm2.

Fig. 9(b) shows the block's connectivity used to model the negative feedback between p53 and Mdm2. First, we program the gene regulatory (block 1) model to behave as an activator (Fig. 3(a)). Block 5 generates a voltage V_{p53} through a simple RC circuit which models the level of the protein p53. Second, the outputs of block 2 (Translation-Transcription) and block 5 are inserted to block 6, which models the dynamics of the Michaels–Menten equation and captures the binding between p53 and mdm2. This block can be implemented as a translinear circuit as given in [3], [19] or as KVL/KCL circuit as shown

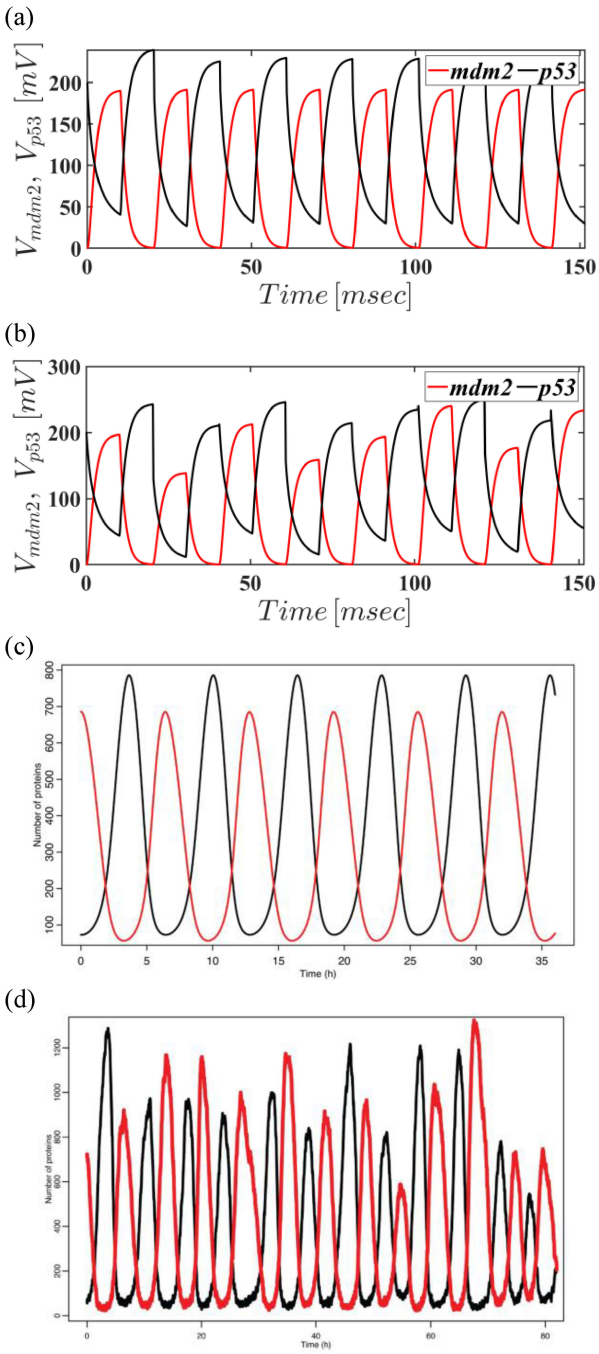

Fig. 10. MATLAB simulation results of the negative feedback interaction between p53 and mdm2 in cancer pathways. (a) Deterministic model and (b) stochastic model. (c-d) Simulation results of the deterministic and stochastic model in [44], respectively; p53 is in black and MDM2 is in red.
Source: G. B. Leenders and J. A. Tuszynski [52]. Copyright 2019 by Leenders and Tuszynski.

in Fig. 3. Then, the output of block 6, which is the free p53, is converted to programming pulses (N_P) through the block 4 and returned in a feedback loop to block 1 to act as an activator. The control block runs the network in reading and programming modes and switches between three states as shown in Fig. 9(c).

When the system is in reading mode (state 1, state 2, state 3 or state 4), at the beginning switches $S_2,\ S_3,\ S_4$ are open and S_1 is closed. Block 1 determines the promoter activity, which is high or low if the level of p53 is high (state 4) or low if the level of p53 is low (state 3). At the same time, block 5 generates the protein p53 (V_{p53}) through a simple RC circuit. Then, switch S_3 closes and the steady state outputs of block 2 (V_{mdm2}) and block 5 (V_{p53}) are inserted to block 6. When the system switches to programming mode (state 5), the switches $S_1,\ S_3$ are open and $S_2,\ S_4$ are closed. The output of block 6 (free p53 - $V_{p53_{free}}$), which acts as an activator for mdm2, is converted to programming pulses (N_{p53}) through block 4. These programming pulses set the memristance of M_{p53} in block 1. If the level of free p53 is high, M_{p53} is programmed to high resistance. On the other hand, if the level of free p53 is low, M_{p53} is programmed to low resistance. In addition, the memristor M_R is programmed to high $(Bias =' 1')$ if a high level of RNAp is bound to the promoter or to low resistance $(Bias =' 0')$ if the basal level RNAp is bound to the promoter. In our model, a high level of RNAp binds the promoter if the level of free p53 is high. In addition to the bias pulse, a stochastic number of pulses (N_{RNAp}) can be generated and added to include stochastics in the network as shown in Fig. 8(c). In this model, the reading time was chosen to be 100x the programming time (Fig. 9(c)) to maintain continuous operation of the circuits (programming time is 10 μsec and reading time is 1 msec).

For the simulation of this system, we set the total number of DNA binding sites that can bind p53 to $D_T = |200\text{ mV}|$. The memristance $M_{P53} \in [2\text{ K}\Omega - 100\text{ K}\Omega]$, where $M_R = 2\,\text{K}\Omega$ represents a basal level of the free p53 and $M_R = 100\text{ K}\Omega$ represents the maximum level of free p53. The dissociation constant for the p53 binding was chosen to be $K = 10\text{ K}\Omega$, the transconductance $g_{m_0} = 150\ \mu\text{S}$, and the gain of block 2 $A_{mRNA} = 1$ and $A_{Protein} = 3$. The transfer function of block 4 ensures that the maximum value of p53 is converted to $N_{p53} = 100$, and the pulse width T_P ensures that $N_{p53} = 100$ sets the memristance to the boundary value R_{OFF}. The current source which represents the maximum generated level of p53 is set to $I_{p53_{Total}} = 200$ mV, and $\tau = R_{p53} \cdot C_{p53}$ was chosen such that V_{P53} reaches steady state quickly.

Fig. 10(a-b) show the deterministic and stochastic simulation results of our model, respectively. Fig. 10(c-d) show the corresponding results from the model presented in [52]. It can be seen that our simulations are compatible with the biological mathematical models that have been developed to explain p53-mdm2 oscillations [52], [54].

VI. Conclusion

We demonstrated the analogies between memristive devices and biochemical reactions at the nanoscale level and showed that such devices can capture the non-linear and stochastic behavior of biochemical reactions. Both systems are non-linear and controlled by time-dependent internal state variables which set the fraction between two boundary states. Programming pulses affect the memristor state similarly to the way enzyme concentration affects biochemical reactions. The time to form a new complex and the delay time of switching memristors

both follow a Poisson distribution. In accordance with the aforementioned analogies and similarities, memristor-based circuits were designed to model processes within a living cell, including induction by small molecules, activation, and repression by transcription factors, hybrid promoters, cooperative binding, and transcriptional and translational regulation of gene expression. Two genetic circuits, the delay induced-oscillator and negative feedback interaction of p53-mdm2 in the p53 pathway, were modeled and simulated as a proof-of-concept. The capability of the memristor-based circuit to capture the analog behavior of biochemical reactions while digitally controlling the flow of signals within the circuits simplifies the design and sheds light on the inner mechanisms.

Several works in the field of cytomorphic circuits [3], [18], [19], [21], [22] have quantitatively mapped the exact chemical differential equations to current-mode circuits. The simulation of a biological system with this approach is carried out by solving the differential equation using analog circuits. The accuracy of the results is a function of the accuracy of the mathematical models and that of the analog circuits. Since biological systems are non-linear, large-scale, stochastic, and very complex, the mathematical models that describe them will not have perfect accuracy. It is moreover almost impossible to construct all the quantitative models and complete their verification and validation. As for the accuracy of the analog circuits, these generally suffer from mismatches as well as process and temperature variations. In addition, for a relatively low number of molecules, the cellular noise in genetic circuits might be high enough such that it masks the signal (noise higher than signal). In that case, the quantitative model will provide no additional information. Therefore, when modeling large-scale gene networks, tissues and organs, qualitative (behavioral) mapping, including stochastics, may be sufficient.

In our future work, we intend to compare the circuits with biological experimental data and develop more advanced models. In addition, we will use the memristor-based circuits to build an accelerator for modeling large-scale biochemical reactions and biological pathways. We will exploit the non-linearity of the memristive devices and the properties of intrinsic stochastic memristor-based circuits to build qualitative models of large-scale biological systems. The biological pathways will be modeled as multi-state systems that perform internal stochastic analog computation at the DNA level and exchange information via digital signals at the protein level.

To build such an accelerator, multi-state memristors are needed. Filamentary RRAMs [45] exhibit promising features for designing cytomorphic circuits: speed, scalability to the nanometer regime, and ultra-low power consumption. The underlying metal-insulator–metal structure is simple, compact, CMOS-compatible, and highly scalable. Filamentary RRAM requires only metal-oxides such as HfOx, AlOx, TaOx films, which are already in use in CMOS fabs. The multi-level has been demonstrated in most of these materials. The filament formation/completion process is inherently abrupt. The switching is achieved by moving only a handful of atomic defects; therefore, large variability through Poissonian statistics ('shot noise') is present. This internal stochasticity can be used to emulate noise in gene expression, as an alternative to programming the device with a random number of pulses. Other non-volatile memories such as phase-change memory [55], conductive-bridging RAM [56], and floating gate transistors can also be used in the design the cytomorphic circuits.

Finally, we expect that the proposed models and circuits will lead to the design of energy-efficient and noise-tolerant cell-inspired electronic circuits. Such circuits will have a direct impact on the fields of synthetic and system biology.

REFERENCES

[1] D. Endy and R. Brent, "Modelling cellular behaviour," *Nature*, vol. 409, no. 6818, pp. 391–395, Jan. 2001.

[2] M. Schwehm, "Fast stochastic simulation of metabolic networks," in *Proc. German Conf. Bioinf.*, 2001, pp. 14–17.

[3] R. Sarpeshkar, *Ultra Low Power Bioelectronics: Fundamentals, Biomedical Applications, and Bio-Inspired Systems*. Cambridge, U.K.: Cambridge Univ. Press, 2010.

[4] U. Alon, *An Introduction to Systems Biology: Design Principles of Biological Circuits*. London, U.K.: Chapman and Hall/CRC, 2006.

[5] D. T. Gillespie, "Exact stochastic simulation of coupled chemical reactions," *J. Phys. Chem.*, vol. 81, no. 25, pp. 2340–2361, 1977.

[6] M. A. Gibson and J. Bruck, "Efficient exact stochastic simulation of chemical systems with many species and many channels," *J. Phys. Chem. A*, vol. 104, no. 9, pp. 1876–1889, 2000.

[7] D. T. Gillespie, "Approximate accelerated stochastic simulation of chemically reacting systems," *J. Chem. Phys.*, vol. 115, no. 4, pp. 1716–1733, 2001.

[8] D. T. Gillespie, "Stochastic simulation of chemical kinetics," *Annu. Rev. Phys. Chem.*, vol. 58, no. 1, pp. 35–55, 2006.

[9] M. Prokopenko, F. Boschetti, and A. J. Ryan, "An information-theoretic primer on complexity, self-organization, and emergence," *Complexity*, vol. 15, no. 1, pp. 11–28, 2009.

[10] V. Balaban, S. Lim, G. Gupta, J. Boedicker, and P. Bogdan, "Quantifying emergence and self-organisation of Enterobacter cloacae microbial communities," *Sci. Rep.*, vol. 8, no. 1, pp. 1–9, 2018.

[11] H. Koorehdavoudi and P. Bogdan, "A statistical physics characterization of the complex systems dynamics: Quantifying complexity from spatio-temporal interactions," *Sci. Rep.*, vol. 6, pp. 1–13, 2016.

[12] M. Niazi and A. Hussain, "Agent-based tools for modeling and simulation of self-organization in peer-to-peer, ad hoc, and other complex networks," *IEEE Commun. Mag.*, vol. 47, no. 3, pp. 166–173, Mar. 2009.

[13] B. Marr, S. Brink, P. Hasler, and D. V. Anderson, "A reconfigurable, analog system for efficient stochastic biological computation," in *Proc. IEEE Biomed. Circuits Syst. Conf.*, 2008, pp. 293–296.

[14] K. Sumiyoshi, K. Hirata, N. Hiroi, and A. Funahashi, "Acceleration of discrete stochastic biochemical simulation using GPGPU," *Front. Physiol.*, vol. 6, pp. 1–10, 2015.

[15] F. Alibart *et al.*, "An organic nanoparticle transistor behaving as a biological spiking synapse," *Adv. Funct. Mater.*, vol. 20, no. 2, pp. 330–337, Jan. 2010.

[16] G. K. Ackers, A. D. Johnson, and M. A. Shea, "Quantitative model for gene regulation by lambda phage repressor.," *Proc. Natl. Acad. Sci.*, vol. 79, no. 4, pp. 1129–1133, 1982.

[17] R. Sarpeshkar, "Analog synthetic biology," *Philos. Trans. R. Soc. A Math. Phys. Eng. Sci.*, vol. 372, 2014, Art. no. 20130110.

[18] R. Daniel, S. S. Woo, L. Turicchia, and R. Sarpeshkar, "Analog transistor models of bacterial genetic circuits," in *Proc. IEEE Biomed. Circuits Syst. Conf.*, 2011, pp. 333–336.

[19] S. Mandal and R. Sarpeshkar, "Log-domain circuit models of chemical reactions," in *Proc. IEEE Int. Symp. Circuits Syst.*, 2009, pp. 2697–2700.

[20] S. Mandal and R. Sarpeshkar, "Circuit models of stochastic genetic networks," in *Proc. IEEE Biomed. Circuits Syst. Conf.*, 2009, no. 2, pp. 109–112.

[21] S. S. Woo, J. Kim, and R. Sarpeshkar, "A cytomorphic chip for quantitative modeling of fundamental bio-molecular circuits," *IEEE Trans. Biomed. Circuits Syst.*, vol. 9, no. 4, pp. 527–542, Aug. 2015.

[22] S. S. Woo, J. Kim, and R. Sarpeshkar, "A digitally programmable cytomorphic chip for simulation of arbitrary biochemical reaction networks," *IEEE Trans. Biomed. Circuits Syst.*, vol. 12, no. 2, pp. 360–378, Apr. 2018.
[23] J. Kim, S. S. Woo, and R. Sarpeshkar, "Fast and precise emulation of stochastic biochemical reaction networks with amplified thermal noise in silicon chips," *IEEE Trans. Biomed. Circuits Syst.*, vol. 12, no. 2, pp. 379–389, Apr. 2018.
[24] L. O. Chua, "Memristor—The missing circuit element," *IEEE Trans. Circuit Theory*, vol. 18, no. 5, pp. 507–519, Sep. 1971.
[25] D. B. Strukov, G. S. Snider, D. R. Stewart, and R. S. Williams, "The missing memristor found," *Nature*, vol. 453, no. 7191, pp. 80–83, 2008.
[26] S. H. Jo, K. H. Kim, and W. Lu, "High-density crossbar arrays based on a Si memristive system," *Nano Lett*., vol. 9, no. 2, pp. 870–874, 2009.
[27] S. H. Jo, T. Chang, I. Ebong, B. B. Bhadviya, P. Mazumder, and W. Lu, "Nanoscale memristor device as synapse in neuromorphic systems," *Nano Lett*., vol. 10, no. 4, pp. 1297–1301, 2010.
[28] T. Tuma, A. Pantazi, M. Le Gallo, A. Sebastian, and E. Eleftheriou, "Stochastic phase-change neurons," *Nat. Nanotechnol.*, vol. 11, no. 8, pp. 693–699, May 2016.
[29] D. Querlioz, W. S. Zhao, P. Dollfus, J. O. Klein, O. Bichler, and C. Gamrat, "Bioinspired networks with nanoscale memristive devices that combine the unsupervised and supervised learning approaches," in *Proc. IEEE/ACM Int. Symp. Nanoscale Archit.*, 2012, pp. 203–210.
[30] J. Borghetti, G. S. Snider, P. J. Kuekes, J. J. Yang, D. R. Stewart, and R. S. Williams, "Memristive switches enable stateful logic operations via material implication," *Nature*, vol. 464, no. 7290, pp. 873–876, 2010.
[31] Y. V. Pershin and M. Di Ventra, "Practical approach to programmable analog circuits with memristors," *IEEE Trans. Circuits Syst. I Regul. Pap.*, vol. 57, no. 8, pp. 1857–1864, Aug. 2010.
[32] H. Jiang *et al.*, "A novel true random number generator based on a stochastic diffusive memristor," *Nat. Commun.*, vol. 8, no. 1, 2017, Art. no. 882.
[33] T. Zhang *et al.*, "High-speed true random number generation based on paired memristors for security electronics," *Nanotechnology*, vol. 28, no. 45, Oct. 2017, Art. no. 455202.
[34] H. A. Hanna, L. Danial, S. Kvatinsky, and R. Daniel, "Modeling biochemical reactions and gene networks with memristors," in *Proc. IEEE Biomed. Circuits Syst. Conf.*, 2018, pp. 1–4.
[35] H. A. Hanna, L. Danial, S. Kvatinsky, and R. Daniel, "Memristors as artificial biochemical reactions in cytomorphic systems," in *Proc. IEEE Int. Conf. Sci. Elect. Eng.*, 2018, no. 2, pp. 1–5.
[36] R. Daniel, J. R. Rubens, R. Sarpeshkar, and T. K. Lu, "Synthetic analog computation in living cells," *Nature*, vol. 497, no. 7451, pp. 619–623, 2013.
[37] K. A. Boahen and A. G. Andreou, "A contrast sensitive silicon retina with reciprocal synapses," in *Proc. 4th Int. Conf. Neural Inf. Process. Syst.*, 1991, pp. 764–772.
[38] J. A. Bell, *General Chemistry*, 3rd ed., vol. 284, no. 5751. Chelmsford, Massachusetts, US: Courier Corporation, 1980.
[39] S. Kvatinsky, M. Ramadan, E. G. Friedman, and A. Kolodny, "VTEAM: A general model for voltage-controlled memristors," *IEEE Trans. Circuits Syst. II Express Briefs*, vol. 62, no. 8, pp. 786–790, Aug. 2015.
[40] M. D. Pickett *et al.*, "Switching dynamics in titanium dioxide memristive devices," *J. Appl. Phys.*, vol. 106, no. 7, 2009, Art. no. 074508.
[41] D. B. Strukov and R. S. Williams, "Exponential ionic drift: Fast switching and low volatility of thin-film memristors," *Appl. Phys. A Mater. Sci. Process.*, vol. 94, no. 3, pp. 515–519, 2009.
[42] S. H. Jo, K. H. Kim, and W. Lu, "Programmable resistance switching in nanoscale two-terminal devices," *Nano Lett*., vol. 9, no. 1, pp. 496–500, 2009.
[43] R. Naous, M. Al-Shedivat, and K. N. Salama, "Stochasticity modeling in memristors," *IEEE Trans. Nanotechnol.*, vol. 15, no. 1, pp. 15–28, Jan. 2016.
[44] L. Danial, N. Wainstein, S. Kraus, and S. Kvatinsky, "DIDACTIC: A data-intelligent digital-to-analog converter with a trainable integrated circuit using memristors," *IEEE J. Emerg. Sel. Topics Circuits Syst.*, vol. 8, no. 1, pp. 146–158, Mar. 2018.
[45] R. S. Cox, M. G. Surette, and M. B. Elowitz, "Programming gene expression with combinatorial promoters," *Mol. Syst. Biol.*, vol. 3, pp. 1–5, 2007.
[46] R. S. Cox, M. G. Surette, and M. B. Elowitz, "Programming gene expression with combinatorial promoters," *Mol. Syst. Biol.*, vol. 3, no. 1, p. 145, 2007.
[47] S. Shin, K. Kim, and S. M. Kang, "Memristor-based fine resolution programmable resistance and its applications," in *Proc. Int. Conf. Commun., Circuits Syst.*, 2009, pp. 948–951.
[48] E. M. Ozbudak, M. Thattai, I. Kurtser, A. D. Grossman, and A. Van Oudenaarden, "Regulation of noise in the expression of a single gene," *Nat. Genet.*, vol. 31, no. 1, pp. 69–73, 2002.
[49] B. B. Kaufmann and A. van Oudenaarden, "Stochastic gene expression: From single molecules to the proteome," *Curr. Opin. Genet. Dev.*, vol. 17, no. 2, pp. 107–112, 2007.
[50] A. Eldar and M. B. Elowitz, "Functional roles for noise in genetic circuits," *Nature*, vol. 467, p. 167, Sep. 2010.
[51] J. Stricker, S. Cookson, M. R. Bennett, W. H. Mather, L. S. Tsimring, and J. Hasty, "A fast, robust and tunable synthetic gene oscillator," *Nature*, vol. 456, no. 7221, pp. 516–519, 2008.
[52] G. B. Leenders and J. A. Tuszynski, "Stochastic and deterministic models of cellular p53 regulation," *Front. Oncol.*, vol. 3, pp. 1–16, 2013.
[53] W. Mather, M. R. Bennett, J. Hasty, and L. S. Tsimring, "Delay-induced degrade-and-fire oscillations in small genetic circuits," *Phys. Rev. Lett.*, vol. 102, no. 6, pp. 1341–1356, 2009.
[54] N. Geva-Zatorsky *et al.*, "Oscillations and variability in the p53 system," *Mol. Syst. Biol.*, vol. 2, 2006, Art. no. 0033.
[55] S. Raoux *et al.*, "Phase-change random access memory: A scalable technology," *IBM J. Res. Dev.*, vol. 52, no. 4–5, pp. 465–479, 2008.
[56] M. N. Kozicki, M. Park, and M. Mitkova, "Nanoscale memory elements based on solid-state electrolytes," *IEEE Trans. Nanotechnol.*, vol. 4, no. 3, pp. 331–338, May 2005.

Hanna Abo Hanna received the B.Sc. degree in electrical engineering in 2017 and the M.Sc. degree in bio-medical engineering from the Technion – Israel Institute of Technology, Haifa, Israel. From 2015 to 2017, he worked as Electrical Verification Student with Intel. He is currently a Designer with the Analog Mixed Signal team at Apple, Haifa, Israel. He won the planning and budgeting committee of the Israel council for higher education (VATAT) fellowship for minority excellent students. His main research interests are analog and mixed-signal circuits using emerging memory devices, cytomorphic and neuromorphic circuits and bio-inspired systems.

Loai Danial received the B.Sc. degree in electrical engineering from the Technion–Israel Institute of Technology, Haifa, Israel, in 2014. He is currently working toward the Ph.D. degree with the Andrew and Erna Viterbi Faculty of Electrical Engineering, Technion–Israel Institute of Technology, Haifa, Israel. From 2013 to 2016, he was with IBM labs as a Hardware Research Student. His current research combines interdisciplinary interests of data converters, machine learning, biology, and mixed-signal systems using emerging memory devices. He received the 2017 Hershel Rich Technion Innovation Award, the Israeli Planning and Budgeting Committee Fellowship, the Andrew and Erna Finci Viterbi Graduate Fellowship's award, and the Best Poster Paper Award at a Nature Conference on Neuromorphic Computing.

Shahar Kvatinsky received the B.Sc. degree in computer engineering and applied physics and the MBA degree from The Hebrew University of Jerusalem, Jerusalem, Israel, in 2009 and 2010, respectively, and the Ph.D. degree in electrical engineering from the Technion – Israel Institute of Technology, Haifa, Israel, in 2014. He is an Associate Professor with the Andrew and Erna Viterbi Faculty of Electrical Engineering, Technion – Israel Institute of Technology. From 2006 to 2009, he was a Circuit Designer with Intel. From 2014 and 2015, he was a Postdoctoral Research Fellow with Stanford University. His current research interests focus on circuits and architectures with emerging memory technologies and design of energy efficient architectures. He is an Editor for *Microelectronics Journal*. He was the recipient of numerous awards: the 2019 Krill Prize for Excellence in Scientific Research, 2015 IEEE Guillemin-Cauer Best Paper Award, 2015 Best Paper of Computer Architecture Letters, Viterbi Fellowship, Jacobs Fellowship, ERC starting grant, the 2017 Pazy Memorial Award, the 2014 and 2017 Hershel Rich Technion Innovation Awards, 2013 Sanford Kaplan Prize for Creative Management in High Tech, 2010 Benin prize, and seven Technion excellence teaching awards.

Ramez Daniel received the B.Sc. degree in electrical engineering from Technion - Israel Institute of Technology, Haifa, Israel, in 2001, and the M.Sc. and Ph.D. degrees in electrical engineering from Tel Aviv University, Tel Aviv, Israel, in 2010. He is an Assistant Professor leading the Synthetic Biology and Bioelectronics group with the Department of Biomedical Engineering, Technion - Israel Institute of Technology. From 2000 to 2006, he was with Tower Semiconductor as a Device/Design Engineer and was a Postdoctoral Research Fellow with Massachusetts Institute of Technology (MIT) from 2010 to 2014. During his work with MIT, he has pioneered a new approach to design biological circuits called "analog genetic circuits," which was published in Nature Journal. He won several awards and prizes (Leader in Science and Technology young academic chair, MAOF Fellowship for new faculty members, VATAT Fellowship for Ph.D. Study, Cum Laude for M.Sc. Study). His current research interests focus on synthetic computation in living cells, bioelectronics and bioinspired technology for biomedical and biotechnology applications.